crystals were evaluated by means of X-ray diffraction (XRD) measurement, Fourier-transform infrared (FT-IR) spectroscopy, and scanning electron microscope (SEM) observation.

2. EXPERIMENTAL DETAILS

2.1. Materials

$Ca(OH)_2$ was prepared by the hydrolysis of calcium oxide, which was obtained by calcination of alkaline-analysis-grade calcium carbonate ($CaCO_3$; Wako Pure Chemical Industries, Ltd., Osaka, Japan) at 1050 °C for 3 h. PAA (weight-average molecular weight: 15,000) used as a polymeric stabilizer was purchased from Sigma-Aldrich Co., MO, USA. Other materials were reagent grade and purchased from Nacalai Tesque Inc., Kyoto, Japan. Milli-Q water with a specific resistance of 18.2×10^6 Ω · cm was used (Millipore Corp., MA, USA).

2.2. Calcination of HAp Particles

Starting HAp particles with low crystallinity were prepared by a modified emulsion system at 25 °C using $Ca(OH)_2$ and potassium dihydrogen phosphate, according to the previous articles.[6,7] The particles prepared was centrifugally washed with water and redispersed in water (solid content: 5 wt%). The calcination procedure of HAp particles with the anti-sintering agent is sketched in Figure 1. An amount of PAA, approximately equal in weight to the HAp particles, was dissolved in water at 1.0 wt%, and the pH of the PAA *aq.* was adjusted to 10.0. The PAA *aq.* was added in the HAp dispersion, and the dispersion was ultrasonicated for 5 min. An excess amount of calcium ions was added to the dispersion in the form of a saturated $Ca(OH)_2$ *aq.* ($Ca(OH)_2$/COOH in PAA = 1/1 molar ratio) to precipitate poly(acrylic acid, calcium salt) (PAA-Ca) onto the HAp particles. The resultant HAp/PAA-Ca mixture was filtered, dried at 80 °C for 2 h under reduced pressure, and calcined at 800 °C for 1 h at a heating rate of 10 °C/min. Calcination was carried out in a horizontal furnace with an alumina tube in air. In order to remove the thermal decomposed product of PAA-Ca, CaO, after calcination, the mixture was centrifugally washed with 100 mM NH_4NO_3 *aq.* under N_2 to reduce the formation of $CaCO_3$ by the reaction between calcium ion and carbon dioxide in air, until the pH of the aqueous dispersion decreased to almost 7.0, and then washed further with water three times. To investigate the effect of the anti-sintering agent, the HAp particles were calcined with the same procedure, but without adding PAA and $Ca(OH)_2$.

2.3. Measurements

Identification of the product was conducted by XRD measurement (RAD-X; Rigaku International Co., Tokyo, Japan) with CuK_α radiation, and diffuse reflectance FT-IR spectroscopy (Spectrum One; Perkin-Elmer Inc., MA, USA). The size and morphology of the HAp crystals were observed by SEM (JSM-6301F; JEOL Ltd., Tokyo, Japan). The Ca/P atomic ratio of each HAp was measured by inductively coupled plasma-atomic emission spectrometry (ICP-AES: SPS4000; Seiko Instrument Inc., Chiba, Japan). Calcium and phosphorus standard solutions for ICP-AES were purchased from Kanto Chemical Co., Inc., Tokyo, Japan.

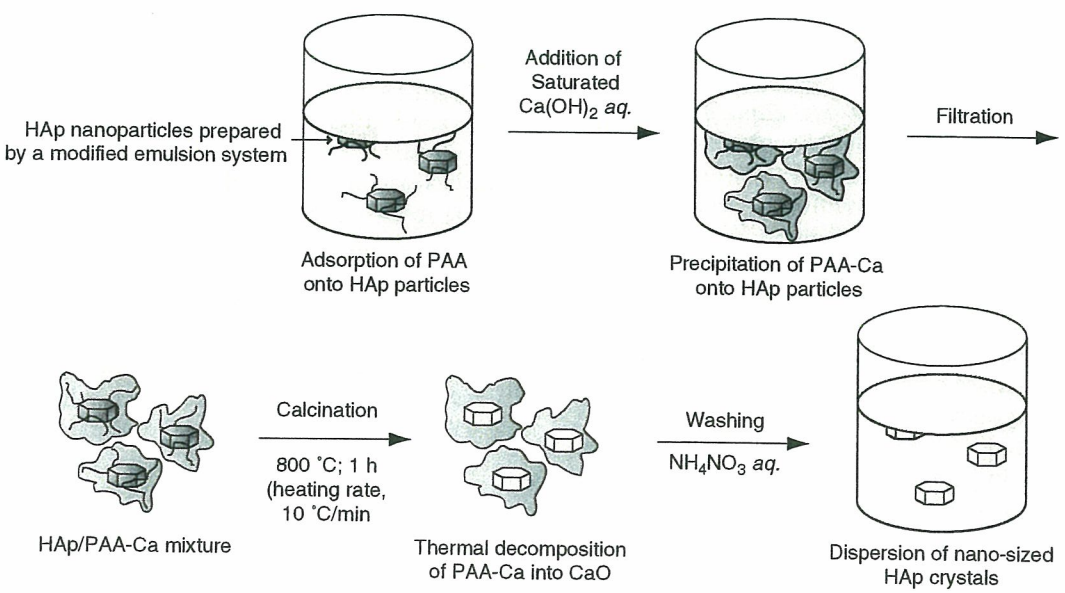

Fig. 1. A schematic model for the fabrication of nano-sized crystals of hydroxyapatite by calcination with an anti-sintering agent surrounding the crystals and subsequent removal of the agent.

RESEARCH ARTICLE

3. RESULTS AND DISCUSSION

In order to surround the particles with the anti-sintering agent, PAA was adsorbed on the surfaces of the HAp particles in an aqueous medium. PAA can adsorb on HAp surfaces,[18–19] and thus act as a polymeric dispersant to prevent flocculation of HAp particles in an aqueous medium. An addition of calcium ions into an aqueous PAA solution under alkaline condition induces precipitation of PAA-Ca. Accordingly, when $Ca(OH)_2$ *aq.* is added to the PAA-stabilized HAp dispersion, PAA-Ca would precipitate onto the surfaces of the HAp particles. The PAA-Ca presumably acts as an anti-sintering agent, because there is no contact among the HAp particles by surrounding them with PAA-Ca and its thermally decomposed product, CaO, during calcination.

First, the influence of PAA-Ca on the crystal phase and composition of HAp were investigated. Figure 2(a) shows the XRD profile of the HAp particles after calcination with PAA-Ca. From the profile, highly crystallized HAp was detected, and no other calcium phosphate phases such as tricalcium phosphate could be detected. The Ca/P ratio of the HAp calcined with PAA-Ca was 1.58 (1.56 in the case of the HAp calcined without additives), indicating the formation of calcium-deficient HAp with high crystallinity after calcination with PAA-Ca.

In the FT-IR spectrum shown in Figure 2(b), the absorption bands at 603/572 and 474 cm^{-1} are respectively attributed to $\nu_4PO_4^{3-}$ and $\nu_2PO_4^{3-}$ in crystalline HAp. Absorptions at 1092/1045 and 963 cm^{-1} are respectively attributed to $\nu_3PO_4^{3-}$ and $\nu_1PO_4^{3-}$. The sharp absorptions of OH stretching and deformation vibrations at 3573 and 632 cm^{-1} indicate that the material exhibits high crystallinity after calcination. Bands at 1456/1413 and 877 cm^{-1}, attributed to CO_3^{2-} substituting phosphate positions in the HAp lattice.[20] The carbonate ion should be from atmospheric carbon dioxide during the preparation of the original HAp particles and from carbon dioxide generated by thermal decomposition of PAA-Ca during calcination.

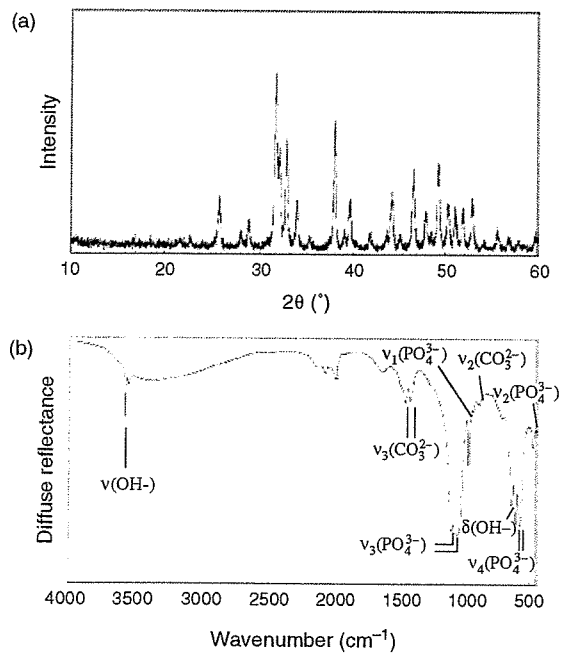

Fig. 2. X-ray diffraction pattern (a) and FT-IR spectrum (b) of HAp crystals calcined at 800 °C for 1 h with PAA-Ca surrounding the particles. The thermal decomposed product of PAA-Ca, CaO, was centrifugally washed with an aqueous solution after calcination.

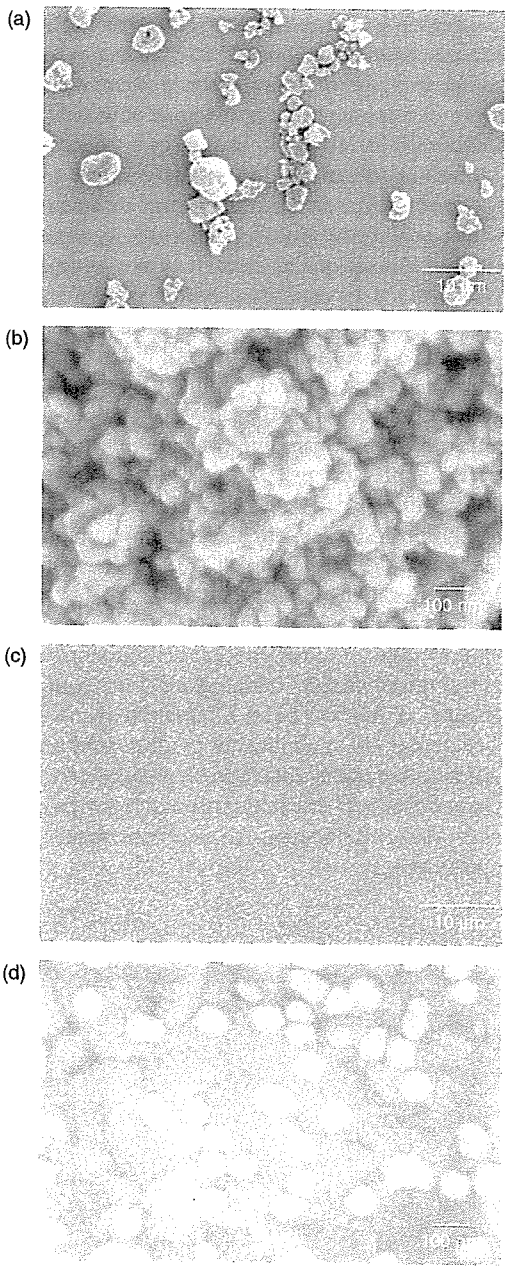

Fig. 3. Lower magnified (a, c) and higher magnified (b, d) SEM photographs of HAp crystals calcined without additives (a, b) and with PAA-Ca (c, d).

RESEARCH ARTICLE

It should be noted that peak at 3644 cm^{-1} due to the stretching of OH in $Ca(OH)_2$ and the peaks at 1453/1415 cm^{-1} corresponding to the CH_2 and CH bending mode of the PAA chain were not found, suggesting complete removal of the anti-sintering agent by the thermal decomposition and the centrifugal washing with water. A small peak at 3544 cm^{-1}, which was not observed in the case of calcination without additives, was additionally observed after calcination with PAA-Ca. The origin of the additional peak is under investigation, and will be reported in the near future.

Figure 3 shows the morphologies of the HAp crystals calcined with or without PAA-Ca. Crystals with spherical or irregular morphologies were observed, irrespective of the presence or absence of PAA-Ca as shown in Figures 3(b) and (d). In the case of calcination without additives shown in Figure 3(a) with lower magnification, micron-sized particles consisting of sintered polycrystals were mainly observed, indicating the calcination-induced sintering among the crystals. On the other hand, in the case of the HAp crystals calcined with the anti-sintering agent shown in Figure 3(c), most of the crystals were observed as isolated particles, and the mean size of the particles was around 80 nm. This indicates that sintering among the HAp nanocrystals could be mostly prevented by surrounding them with PAA-Ca prior to calcination.

In summary, calcined HAp nanocrystals were successfully fabricated by calcination with an anti-sintering agent surrounding the particles, followed by removal of the agent. The HAp nanocrystals fabricated here should be suitable for the various applications such as biomaterials, ion exchangers, adsorbents, and catalysts owing to their high dispersibility in liquid media and high thermal and chemical stability. The calcination with an anti-sintering agent should be applicable to other nanoceramic powders, such as alumina, titania, and magnesia, and have significant benefits over existing technologies, because the methods is facile, inexpensive, and amenable to scale-up and processing.

Acknowledgments: We thank Dr. K. Sato of the Advanced Manufacturing Research Institute, National Institute of Advanced Industrial Science and Technology (AIST), for helpful discussions. This work was supported by a Research Grant for Cardiovascular Diseases from the Ministry of Health, Labour, and Welfare, Japan.

References and Notes

1. H. Aoki, Science and Medical Application of Hydroxyapatite, Takayama Press System Center Co., Inc. (1991).
2. W. Suchanek, M. Yashima, M. Kakihana, and M. Yoshimura, *J. Am. Ceram. Soc.* 80, 2805 (1997).
3. C. R. Kothaplli, M. Wei, R. Z. Legeros, and M. T. Shaw, *J. Mater. Sci.: Mater. Med.* 16, 441 (2005).
4. T. Furuzono, K. Sonoda, and J. Tanaka, *J. Biomed. Mater. Res.* 56, 9 (2001).
5. T. Furuzono, S, Yasuda, T. Kimura, S. Kyotani, J. Tanaka, and A. Kishida, *J. Artif. Organs* 7, 137 (2004).
6. T. Furuzono, D. Walsh, K. Sato, K. Sonoda, and J. Tanaka, *J. Mater. Sci. Lett.* 20, 111 (2001).
7. K. Sonoda, T. Furuzono, D. Walsh, K. Sato, and J. Tanaka, *Solid State Ionics* 151, 321 (2002).
8. J. Frenkel, *J. Phys. USSR* 9, 385 (1945).
9. G. C. Kuczynski, *Trans. AIME* 185, 169 (1949).
10. J. E. Barralet, S. M. Best, and W. Bonfield, *J. Mater. Sci.: Mater. Med.* 11, 719 (2000).
11. E. Landi, A. Tampieri, G. Celotti, and S. Sprio, *J. Eur. Ceram. Soc.* 20, 2377 (2000).
12. D. Bernache-Assollant, A. Ababoua, E. Championa, and M. Heughebaertb, *J. Eur. Ceram. Soc.* 23, 229 (2003).
13. S. Somiya, K. Ioku, and M. Yoshimura, *Mater. Sci. Forum* 34–36, 371 (1988).
14. M. Yoshimura, H. Suda, K. Okamoto, and K. Ioku, *J. Mater. Sci.* 29, 3399 (1994).
15. A. D. Papargyris, A. I. Botis, and S. A. Papargyri, *Key Eng. Mater.* 206–213, 83 (2002).
16. J. E. Carless and A. A. Foster, *J. Pharmaceut. Pharmacol.* 18, 697 (1966).
17. M. Wei, A. J. Ruys, B. K. Milthorpe, and C. C. Sorrell, *J. Biomed. Mater. Res.* 45, 11 (1999).
18. D. N. Misra, *J. Dent. Res.* 10, 1418 (1993).
19. Y. Yoshida, B. Van Meerbeek, Y. Nakayama, M. Yoshioka, J. Snauwaert, Y. Abe, P. Lambrechts, G. Vanherle, and M. Okazaki, *J. Dent. Res.* 80, 1565 (2001).
20. W. H. Emerson and E. E. Fisher, *Arch. Oral. Biol.* 7, 671 (1962).

Received: 6 November 2005. Accepted: 13 March 2006.

RESEARCH ARTICLE

Journal of Nanoparticle Research (2006)
DOI 10.1007/s11051-006-9126-1

Calcination of rod-like hydroxyapatite nanocrystals with an anti-sintering agent surrounding the crystals

M. Okada and T. Furuzono*
*Department of Bioengineering, Advanced Medical Engineering Center, National Cardiovascular Center Research Institute, 5-7-1 Fujishirodai, Suita, Osaka, 565-8565, Japan; *Author for correspondence (E-mail: furuzono@ri.ncvc.go.jp)*

Received 10 October 2005; accepted in revised form 4 May 2006

Key words: hydroxyapatite, nanocrystal, calcination, dispersion, thermal decomposition, sintering

Abstract

Sintering-free nanocrystals of calcined hydroxyapatite (HAp) having a rod-like morphology were fabricated by calcination at 800°C for 1 h with an anti-sintering agent surrounding original HAp particles and the agent was subsequently removed after calcination. The original HAp particles having a rod-like morphology with a size ranging from 30 to 80 nm (short axis) and 300 to 500 nm (long axis) were prepared by wet chemical process, and poly(acrylic acid, calcium salt) (PAA-Ca) was used as the anti-sintering agent. In the case of calcination without additives, the mean size of HAp crystals dispersed in an ethanol medium increased by about 4 times and the specific surface area of the crystals exhibited a 25% decrease compared to those of the original HAp particles because of calcination-induced sintering among the crystals. On the other hand, the HAp crystals calcined with the anti-sintering agent, PAA-Ca, could be dispersed in an ethanol medium at the same size as the original particles, and they preserved the specific surface area after calcination. These results indicate that PAA-Ca and/or its thermally decomposed product, CaO, surrounded the HAp particles and protected them against calcination-induced sintering during calcination. The HAp crystals calcined with PAA-Ca showed high crystallinity, and no other calcium phosphate phases could be detected after washing with water.

Introduction

Hydroxyapatite (HAp, $Ca_{10}(PO_4)_6(OH)_2$) is ideal as the main mineral of bones and teeth. Artificially synthesized HAp has been extensively used in a variety of applications, such as biomaterials, ion exchangers, adsorbents, and catalysts by exploiting its biocompatibility and adsorbability with many compounds. However, owing to its mechanical weakness and brittleness (Aoki, 1991; Suchanek et al., 1997), applications of HAp have been confined to those with low mechanical stress. In order to overcome the weakness of HAp, we have recently developed a novel inorganic/organic composite as a soft-tissue compatible material: a flexible silicone elastomer (Furuzono et al., 2001) or a silk fibroin (Furuzono et al., 2004), whose surface was modified with calcined HAp crystals through covalent bonding. The novel composite retained the flexibility of the polymer substrate and showed good tissue adhesion due to the HAp crystals on the surface (Furuzono et al., 2003). Throughout these studies, the HAp crystals were used after calcination at 800°C to reduce *in vivo* sorbability, because a slight inflammatory response was reported in the case of the amorphous HAp

coating on silicone elastomer by pulsed laser deposition (Zabetakis et al., 1994).

HAp nanoparticles can be synthesized in a number of ways, such as wet chemical process (Jarcho et al., 1976; Schmidt, 2000; Cushing et al., 2004), sol–gel process (Masuda et al., 1990; Sanchez & Livage, 1990; Schmidt et al., 1998), and emulsion process (Lim et al., 1996; Sonoda et al., 2002). Among these processes, wet chemical process has been widely used because it is simple and the morphology of the HAp particles can be changed by reaction conditions such as pH, temperature and concentration of reactants or additives (Jarcho et al., 1976; Schmidt, 2000; Cushing et al., 2004). The morphology will affect the adsorption properties of biopolymers such as proteins and the ion-exchange property, because HAp belongs to a hexagonal crystal system and possesses different properties on its *a* and *c* planes (Kawasaki, 1991).

When low-crystallinity HAp nanoparticles synthesized via the above processes are calcined to increase thermal and chemical stability, the particles typically sinter into large agglomerates consisting of polycrystals (Barralet et al., 2000; Landi et al., 2000; Bernache-Assollant et al., 2003). Because sintered HAp polycrystals has poor dispersibility in liquid media and a large size distribution, it is difficult to control the surface morphology (covering ratio by HAp, surface roughness) of the above-mentioned inorganic/organic composite. Hydrothermal treatment of HAp particles in an aqueous medium under high pressure is known to enable the preparation of sintering-free HAp single crystals (Somiya et al., 1988; Yoshimura et al., 1994; Papargyris et al., 2002). However, this treatment generally leads to an increase in crystal size due to Ostwald ripening (Carless & Foster, 1966), and is restricted to laboratory-scale products as it is a high-pressure process.

In our previous article (Okada & Furuzono, 2006), in order to control the surface morphology of the above-mentioned composite, agglomerate-free HAp nanocrystals having a spherical morphology were fabricated by calcination with an anti-sintering agent surrounding the HAp particles and subsequent removal of the agent. That is, there was no contact among the particles during calcination. Original HAp nanoparticles with low crystallinity and a spherical morphology were prepared by a modified emulsion system (Sonoda et al., 2002) at 25°C, and calcined with calcium hydroxide [$Ca(OH)_2$]. $Ca(OH)_2$ was selected as the anti-sintering agent, because $Ca(OH)_2$ does not melt at the calcination temperature (800°C), presumably would not dissolve the HAp, and could be removed by washing with water after calcination.

In this article, original HAp particles having a rod-like morphology prepared by the wet chemical process were calcined with an anti-sintering agent in order to extend the application of calcination with an anti-sintering agent. Poly(acrylic acid) (PAA) was used to surround the HAp particles efficiently with the anti-sintering agent, and the thermal decomposition behavior of the agent during calcination was investigated. Furthermore, the influence of the anti-sintering agent on the crystal phase, composition, and particle size of the HAp crystals was investigated.

The HAp nanocrystals obtained here should be suitable for various applications, such as biomaterials, ion exchangers, adsorbents, catalysts, and dental and orthopedic ultrafine fillers for microporosity owing to their high dispersibility in liquid media and high thermal and chemical stability. Calcination with an anti-sintering agent has potential application to a wide range of calcined nanoceramic powders, such as alumina, titania, and magnesia, and offer significant benefits over existing technologies because the technique is simple, inexpensive, and amenable to scaling-up and processing.

Experimental

Materials

$Ca(OH)_2$ was prepared by the hydrolysis of calcium oxide obtained by calcination of alkaline-analysis-grade calcium carbonate ($CaCO_3$; Wako Pure Chemical Industries, Ltd., Osaka, Japan) at 1050°C for 3 h. A 25% ammonia solution and diammonium hydrogenphosphate [$(NH_4)_2HPO_4$] were purchased from Wako Pure Chemical Industries, Ltd. Guaranteed reagent-grade calcium nitrate tetrahydrate [$Ca(NO_3)_2{\cdot}4H_2O$] and ammonium nitrate [NH_4NO_3] were purchased from Nacalai Tesque Inc., Kyoto, Japan. PAA (weight-average molecular weight: 15,000), used as a

polymeric stabilizer, was purchased from Sigma-Aldrich Co., MO, USA. Milli-Q water with a specific resistance of 18.2×10^6 Ω cm was used (Millipore Corp., MA, USA).

HAp particles

Original HAp particles with a rod-like morphology were prepared by the wet chemical process as follows. 42 mM $Ca(NO_3)_2$ aq. and 100 mM $(NH_4)_2HPO_4$ aq. were prepared, and the pH of each solution was adjusted to 12.5 by adding a 25% ammonia solution. 800 ml of the $Ca(NO_3)_2$ aq. was poured into a 1-l reactor equipped with an inlet of N_2, a reflux condenser, and a half-moon type stirrer. After the temperature in the reactor had been raised to 80°C, 200 ml of the $(NH_4)_2HPO_4$ aq. was added into the reactor at a feeding rate of 20 m/h, and the resultant mixture was stirred for another 10 h at 80°C. The obtained HAp particles were centrifugally washed with water, and re-dispersed in a water medium.

Calcination

The calcination procedure of HAp particles with an anti-sintering agent is sketched in Figure 1. An amount of PAA, approximately equal in weight to the HAp particles, was dissolved in water at 1.0 wt%, and the pH of the PAA aq. was adjusted to 10.0. The PAA aq. was added in the HAp dispersion (solid content, 1.0 wt%), and the dipsersion was ultrasonicated for 5 min. A saturated $Ca(OH)_2$ aq. was added to the dispersion ($Ca(OH)_2$/COOH in PAA = 1/1 molar ratio) to precipitate poly(acrylic acid, calcium salt) (PAA-Ca) onto the HAp particles. The resultant HAp/PAA-Ca mixture was filtered, rinsed with water, and dried at 80°C for 2 h under reduced pressure. The dried HAp/PAA-Ca mixture was placed on an alumina tube in a horizontal furnace at room temperature in air. In order to calcine the mixture, the furnace was heated from room temperature to 800°C at a heating rate of 10°C/min, and the temperature was kept at 800°C for 1 h after the temperature had reached to 800°C. After that, the heater of the furnace was automatically turned-off. The resultant powder after calcination was centrifugally washed with 100 mM NH_4NO_3 aq. until the pH of the aqueous medium decreased to almost 7.0, and then washed with water three times. As a control procedure, the same original HAp particles were calcined without adding PAA and $Ca(OH)_2$.

Thermal decomposition of PAA-Ca

PAA-Ca was precipitated by adding a saturated $Ca(OH)_2$ aq. into PAA aq. at an initial pH of 10.0 in the absence of HAp particles. The precipitation

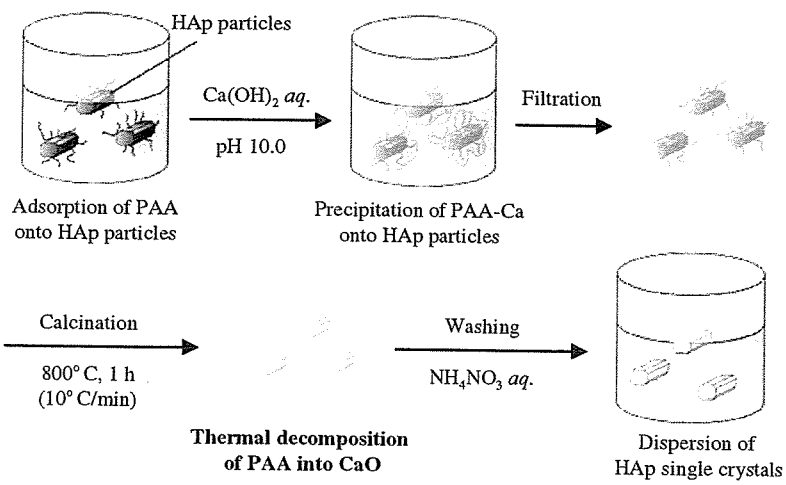

Figure 1. Schematic model for the fabrication of single nanocrystals of hydroxyapatite calcined with an anti-sintering agent and subsequently removing the agent.

was filtered, rinsed with water, and dried at 80°C for 2 h under reduced pressure. The PAA-Ca was calcined at 800°C for 1 h with the same procedure described in the Section 'Calcination'. The thermal decomposition behavior of PAA-Ca was measured by a thermogravimeter (TG; EXSTAR6000 TG/DTA6300, Seiko Instruments Inc., Chiba, Japan). The heating rate for TG measurement was 10°C/min and the temperature range was from 30°C to 1000°C.

Measurements

Identification of the product was conducted by X-ray diffraction (XRD) measurement (RAD-X; Rigaku International Co., Tokyo, Japan) with CuKa radiation, and diffuse reflectance Fourier-transform infrared (FT-IR) spectroscopy (Spectrum One; Perkin–Elmer Inc., MA, USA). The morphology of the HAp crystals was observed by scanning electron microscopy (SEM; JSM-6301F, JEOL Ltd., Tokyo, Japan) and transmission electron microscopy (TEM; JEM-2000 EXII, JEOL Ltd.). The size distribution of the HAp crystals dispersed in an ethanol medium was measured at a 10-ppm concentration by dynamic light scattering (DLS; ELS-8000, Otsuka Electronics Co., Ltd., Kyoto, Japan) at a light-scattering angle of 90°. The Ca/P atomic ratio of each HAp was measured by inductively coupled plasma-atomic emission spectrometry (ICP-AES; SPS4000, Seiko Instrument Inc., Chiba, Japan). Calcium and phosphorus standard solutions for ICP-AES were purchased from Kanto Chemical Co., Inc., Tokyo, Japan. The specific surface area of the particles was measured by the Brunauer–Emmett–Teller (BET) triple-point method with nitrogen adsorption (NOVA1200e, Quantachrome Instruments, FL, USA) after degassing the powder at 100°C under reduced pressure for 10 min. The data resulting from BET measurements are presented as means ± SD for mean (N = 3). Statistical comparisons were performed with the use of a Student's t-test. The level of statistical significance was defined as $p < 0.01$.

Results and discussion

First, in order to check the thermal decomposition behavior of PAA-Ca used as an anti-sintering agent, PAA-Ca was calcined in air at 800°C for 1 h. Figure 2 shows the FT-IR spectra of PAA and PAA-Ca. PAA showed major peaks at 1695 cm^{-1}, corresponding to the C=O stretching of the carboxyl groups and at 1453/1415 cm^{-1}, corresponding to the CH_2 and CH bending mode of the PAA chain (Figure 2a). In the spectrum of the PAA-Ca shown in Figure 2b, the peak at 1695 cm^{-1} decreased and a new peak appeared at 1565/1330 cm^{-1}, corresponding to the stretching mode of ionized carboxyl groups, suggesting the formation of a significant number of Ca–O interactions (Sindhu & Valiyaveettil, 2004). The broad peak around 3600 cm^{-1} in Figure 2b seems to be corresponding to the OH stretching in free COOH or absorbed water, because $Ca(OH)_2$ crystal phase was not observed by XRD. After calcination of PAA-Ca (Figure 2c), new characteristic peaks appeared at 3644 cm^{-1} corresponding to the OH stretching in $Ca(OH)_2$. This indicates that the organic component of PAA-Ca was completely decomposed and PAA-Ca became $Ca(OH)_2$ after calcination. It should be noted that the formation of $Ca(OH)_2$ is favorable because it can be removed by dissolving in an aqueous medium.

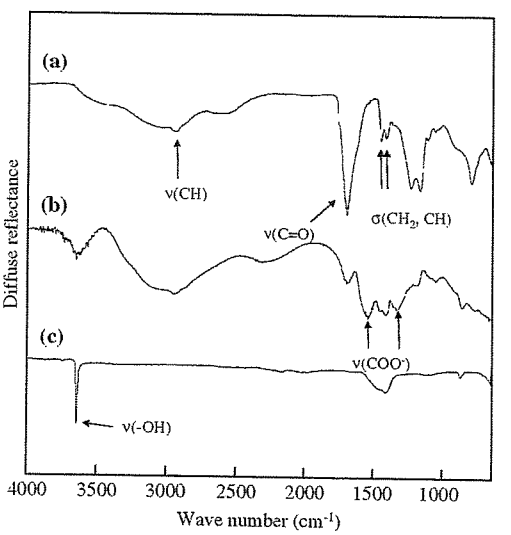

Figure 2. FT-IR spectra of (a) poly(acrylic acid) (PAA); (b) poly(acrylic acid calcium salt) (PAA-Ca) precipitated by adding a saturated $Ca(OH)_2$ aq. in a PAA aqueous solution ($Ca(OH)_2$/COOH in PAA = 1/1 molar ratio); (c) PAA-Ca after calcination at 800°C for 1 h at a heating rate of 10°C/min.

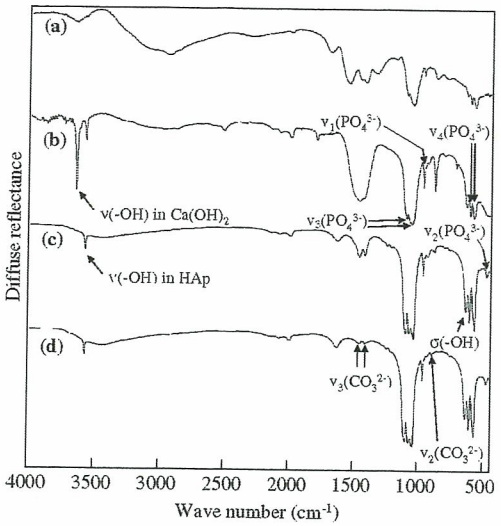

Figure 5. FT-IR spectra of (a) a mixture of HAp particles and PAA-Ca prepared by addition of saturated $Ca(OH)_2$ aq. in PAA-stabilized HAp aqueous dispersion, (b) the HAp/PAA-Ca mixture after calcination at 800°C for 1 h, (c) HAp nanocrystals after washing with water, and (d) HAp crystals after calcination without additives.

603/572 and 474 cm^{-1} are, respectively attributed to $\nu_4PO_4^{3-}$ and $\nu_2PO_4^{3-}$ in crystalline HAp. Absorptions at 1092/1045 and 963 cm^{-1} are, respectively attributed to $\nu_3PO_4^{3-}$ and $\nu_1PO_4^{3-}$. The sharp absorptions of OH stretching and vibration at 3573 and 632 cm^{-1} indicate that the material exhibits high crystallinity (Fowler, 1974; Taylor et al., 2001) after the calcination (Figure 5b–d). In the FT-IR spectrum of the HAp calcined with PAA-Ca followed by washing with water (Figure 5c), a peak at 3644 cm^{-1} due to the stretching of OH in $Ca(OH)_2$ (observed in Figure 5b) disappeared, suggesting removal of $Ca(OH)_2$. Bands at 1456/1413 and 877 cm^{-1}, attributed to CO_3^{2-} substituting phosphate positions in the HAp lattice (Emerson & Fisher, 1962), increased in the case of calcination with PAA-Ca (Figure 5c) as compared to that without additives (Figure 5d). This seems to be due to incorporation of CO_3^{2-} in HAp lattice by the reaction with atmospheric carbon dioxide generated by thermal decomposition of PAA-Ca during calcination. CO_3^{2-} in Figure 5d seems to be incorporated during the wet chemical process and the reaction with CO_2 in air during calcination (Ishikawa et al.,

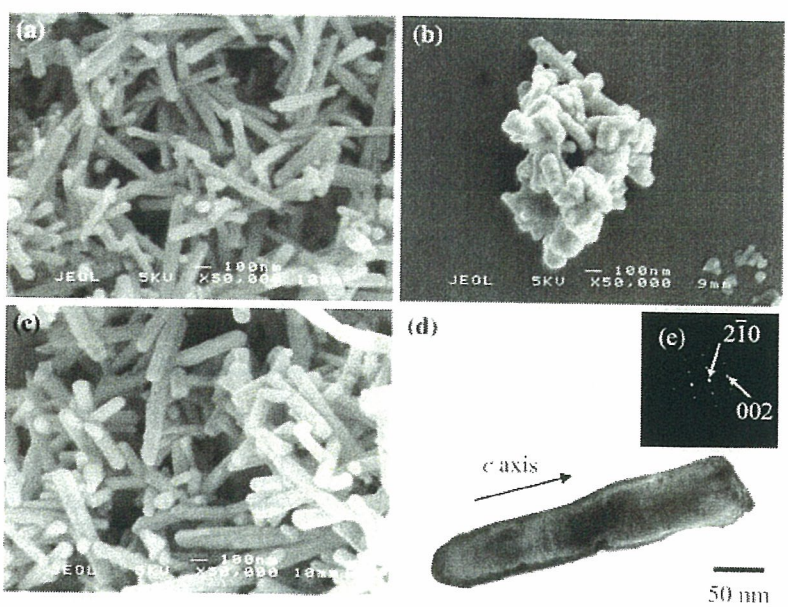

Figure 6. SEM photographs of (a) original HAp particles before calcination, and HAp crystals after calcination (b) without additive and (c) with PAA-Ca. (d) A TEM photograph and (e) the associated electron diffraction pattern of a HAp crystal calcined with PAA-Ca, showing the crystal consisting of a single HAp phase.

The *in situ* thermal decomposition of PAA-Ca during calcination was measured by TG as shown in Figure 3. The TG measurement was conducted at a heating rate of 10°C/min in air. In the case of $CaCO_3$ with a calcite structure (Figure 3a), the weight loss started at 707°C and its weight decreased by 44.2%, which should be due to the detachment of CO_2 molecules (43.9% in weight, calculated from the chemical formula of $CaCO_3$). On the other hand, the weight of PAA-Ca gradually decreased to 87.2% due to the evaporation of absorbed water, and drastically decreased at 516°C to 49.6% with exothermic heat (see Figure 3b: time vs. temperature). This indicates the thermal decomposition of the organic components in PAA-Ca. Another weight loss started at 683°C and 28.1% of its weight remained in the latter stage. The weight loss [(49.6 − 28.1)/49.6×100 = 43.3%] and the starting temperature (683°C) of the latter stage almost corresponded to those of $CaCO_3$ (weight loss, 44.2%; temperature, 707°C). These results indicate that PAA-Ca was decomposed finally into CaO with the detachment of CO_2 molecules during calcination, and $Ca(OH)_2$ observed in Figure 2c was formed by a hydrolysis reaction of a part of CaO with moisture in air, as described in the following equation:

$$\text{PAA-Ca} \xrightarrow{520^\circ\text{C}\sim} CaCO_3 \xrightarrow{680^\circ\text{C}\sim} CaO \xrightarrow{+H_2O} Ca(OH)_2 \quad (1)$$

The rod-like HAp particles prepared by the wet chemical process were calcined with PAA-Ca surrounding the particles (Figure 1). In order to surround the particles with PAA-Ca, first, PAA was adsorbed on the surfaces of the HAp particles in an aqueous medium. PAA can adsorb on the HAp surfaces (Misra, 1993; Yoshida et al., 2001; Bonapasta et al., 2001), and thus act as a polymeric dispersant to prevent flocculation in an aqueous medium. The addition of calcium ions into an aqueous PAA solution induces precipitation of PAA-Ca. Accordingly, when calcium ions are added to the PAA-stabilized HAp dispersion, PAA-Ca precipitates onto the surfaces of the HAp particles. The PAA-Ca presumably acts as an anti-sintering agent, because there is no contact among the HAp particles by surrounding them with PAA-Ca and/or its thermally decomposed product, CaO, during calcination.

In order to investigate the effect of the anti-sintering agent on the crystal phase and composition of HAp, XRD and FT-IR measurements were conducted. The results are shown in Figures 4 and 5. In Figure 4, both the XRD profiles of the particles calcined without additives and those with PAA-Ca showed highly crystalline HAp. It is worth pointing out that other calcium phosphate phases, CaO, and $Ca(OH)_2$ could not be detected from each XRD profile. In the FT-IR spectra shown in Figure 5, the absorption bands at

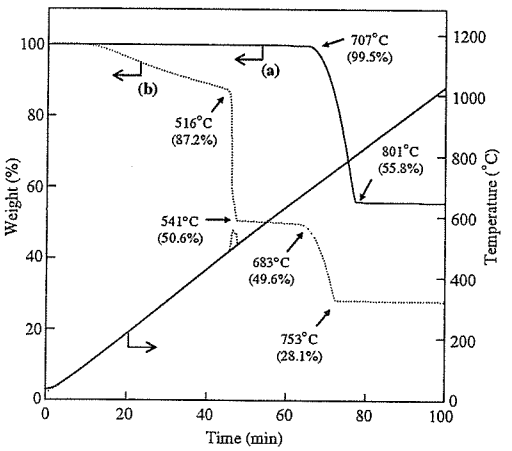

Figure 3. Thermal decomposition behavior of (a; solid line) $CaCO_3$ with calcite structure and (b; dotted line) PAA-Ca at a heating rate of 10°C/min in air.

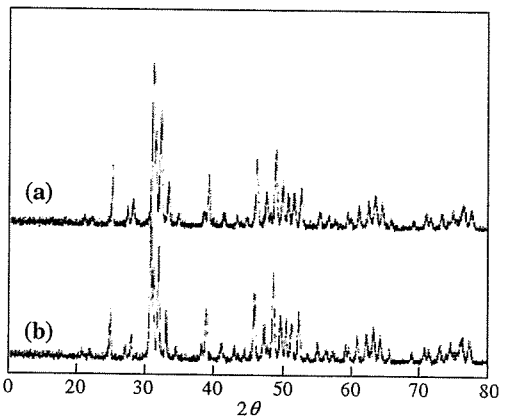

Figure 4. XRD patterns of HAp nanocrystals calcinated (a) without additive and (b) with PAA-Ca at 800°C for 1 h at a heating rate of 10°C/min in air, followed by washing with water.

1991; Cheng et al., 1998). From the ICP-AES measurement, the Ca/P molar ratio of the HAp calcined with PAA-Ca was 1.72, and that without additives corresponded to that of stoichiometric HAp (Ca/P = 1.67). It is worth pointing out that the calcium-rich carbonate-substituted HAp had improved mechanical and biological properties compared to stoichiometric HAp (Gibson & Bonfield, 2002). We have already reported that the HAp nanocrystals, which were calcined with the anti-sintering agent, coated on a poly(ethylene terephthalate) (PET) substrate showed no cell toxicity and an improvement of cell adhesion compared to the unmodified PET substrate (Furuzono et al., 2006).

Figure 6 shows SEM and TEM photographs of the original HAp particles and the calcined HAp crystals. In the SEM photograph of the original HAp particles (Figure 6a), they had a rod-like morphology with a size ranging from 30 to 80 nm (short axis) and 300 to 500 nm (long axis). In the case of calcination without additives, some micron-sized agglomerates of polycrystals were observed, as shown in Figure 6b. On the other hand, in the case of calcination with PAA-Ca, the rod-like morphology was preserved. The higher-magnification TEM image of a particle calcined with PAA-Ca and its electron diffraction pattern (Figure 6d and e, respectively) confirmed that the particle was a single HAp crystal, and the long axis of the crystal was parallel to the *c*-axis of the HAp lattice. Other calcium phosphate phases could not be detected in the inside nor on the surface layer of the HAp crystals in Figure 6d.

The size distribution of HAp crystals and the specific surface area of the crystals are shown in Figures 7 and 8, respectively. The size distribution shown in Figure 7 was measured in an ethanol medium by DLS. In the case of calcination without additives, the mean size (1871 nm) and the specific surface area (15.5 m^2/g) of the crystals were, respectively much larger and smaller than those of the original particles before calcination (mean size, 468 nm; specific surface area, 19.6 m^2/g), which indicate the formation of agglomerates consisting of sintered polycrystals after calcination

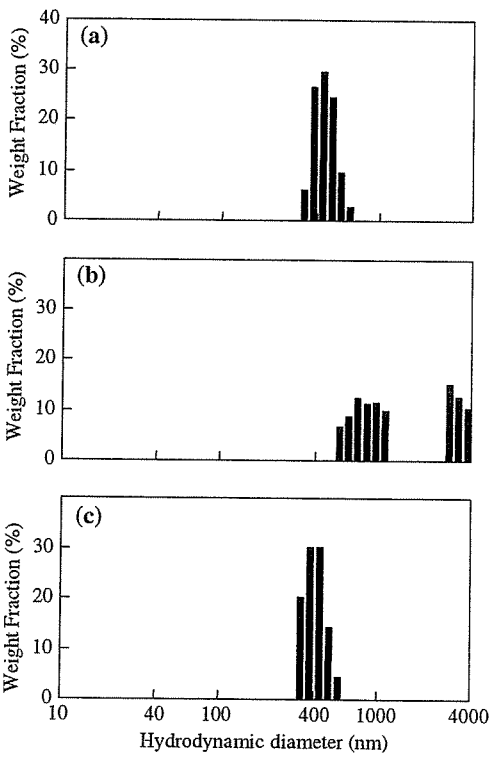

Figure 7. Size distributions of (a) original HAp particles before calcination, and HAp crystals after calcination (b) without additive and (c) with PAA-Ca. The size distributions were measured in ethanol.

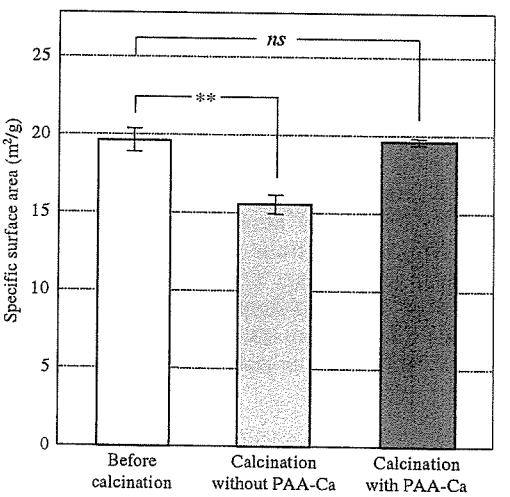

Figure 8. Specific surface areas of (a) original HAp particles, and HAp crystals after calcination (b) without additive and (c) with PAA-Ca. Error bars represent standard deviations of triplicates (**$p < 0.01$).

without additives. In the case of calcination with PAA-Ca, the size distribution (mean size, 430 nm) and the specific surface area (19.6 m^2/g) of the crystals almost corresponded to those of the original particles before calcination, respectively. In addition, the size of the HAp crystals in ethanol was close to the crystallite size in the long axis (300–500 nm) determined from the electron micrographs (Figure 6c). These results indicate that sintering between the HAp nanocrystals could be prevented by PAA-Ca surrounding the crystals prior to calcination.

Conclusion

HAp nanocrystals having a rod-like morphology were calcined at 800°C for 1 h with PAA-Ca used as the anti-sintering agent surrounding the particles, followed by removal of the agent. Although PAA-Ca was thermally decomposed during calcination, the decomposed product, CaO, remained on the particle surface. In the case of calcination without additives, some large agglomerates consisting of sintered polycrystals were observed. On the other hand, the HAp nanocrystals calcined with PAA-Ca showed high dispersibility in liquid media and a large specific surface area due to the anti-sintering effect of PAA-Ca surrounding the particles. Also, the HAp crystals calcined with PAA-Ca showed highly crystallinity, and no other calcium phosphate phases could be detected.

Acknowledgment

We thank Dr. Y. Yokogawa and Dr. K. Sato of the Advanced Manufacturing Research Institute, National Institute of Advanced Industrial Science and Technology (AIST), for helpful discussions. This work was supported by a Research Grant for Cardiovascular Diseases from the Ministry of Health, Labour and Welfare, Japan.

References

Aoki H., 1991. Science and Medical Application of Hydroxyapatite. Takayama Press System Center Co., Inc.

Barralet J.E., S.M. Best & W. Bonfield, 2000. Effect of sintering parameters on the density and microstructure of carbonate hydroxyapatite. J. Mater. Sci. Mater. Med. 11, 719–724.

Bernache-Assollant D., A. Ababoua, E. Championa & M. Heughebaertb, 2003. Sintering of calcium phosphate hydroxyapatite $Ca_{10}(PO_4)_6(OH)_2$ I. Calcination and particle growth. J. Eur. Ceram. Soc. 23, 229–241.

Bonapasta A.A., F. Buda & P. Colombet, 2001. Interaction between Ca ions and poly(acrylic acid) chains in macro-defect-free cements: A theoretical study. Chem. Mater. 13, 64–70.

Carless J.E. & A.A. Foster, 1966. Accelerated crystal growth of sulfathiazole by temperature cycling. J. Pharmaceut. Pharmacol. 18, 697–708.

Cheng Z.H., A. Yasukawa, K. Kandori & T. Ishikawa, 1998. FTIR study on incorporation of CO_2 into calcium hydroxyapatite. J. Chem. Soc. Faraday Trans. 94, 1501–1505.

Cushing B.L., V.L. Kolesnichenko & C.J. O'Connor, 2004. Recent advances in the liquid-phase syntheses of inorganic nanoparticles. Chem. Rev. 104, 3893–3946.

Emerson W.H. & E.E. Fisher, 1962. The infrared absorption spectra of carbonate in calcified tissue. Arch. Oral. Biol. 7, 671–683.

Fowler B.O., 1974. Infrared studies of apatites. I Vibrational assignments for calcium, strontium, and barium hydroxyapatites utilizing isotopic substitution. Inorg. Chem. 13, 194–206.

Furuzono T., A. Kishida & J. Tanaka, 2004. Nano-scaled hydroxyapatite/polymer composite I. Coating of sintered hydroxyapatite particles on poly(γ-methacryloxypropyl trimethoxysilane)-grafted silk fibroin fibers through chemical bonding. J. Mater. Sci. Mater. Med. 15, 19–23.

Furuzono T., K. Sonoda & J. Tanaka, 2001. A hydroxyapatite coating covalently linked onto a silicone implant material. J. Biomed. Mater. Res. 56, 9–12.

Furuzono T., P. Wang, A. Korematsu, K. Miyazaki, M. Oido-Mori, Y. Kowashi, K. Ohura, J. Tanaka & A. Kishida, 2003. Physical and biological evaluations of sintered hydroxyapatite/silicone composite with covalent bonding for a percutaneous implant material. J. Biomed. Mater. Res. B: Appl. Biomater. 65B, 217–226.

Furuzono T., M. Masuda, M. Okada, S. Yasuda, H. Kadono, R. Tanaka & K. Miyatake, 2006. Increase of cell adhesiveness on poly(ethylene terephthalate) fabric by coating of sintered hydroxyapatite nanocrystals for development of an artificial blood vessel. ASAIO J. (in press).

Gibson I.R. & W. Bonfield, 2002. Novel synthesis and characterization of an AB-type carbonate-substituted hydroxyapatite. J. Biomed. Mater. Res. 59, 697–708.

Ishikawa K., Y. Ishikawa & N. Kuwayama, 1991. Preparation of carbonate-bearing hydroxyapatites and their sintering properties. Chem. Express 6, 463–466.

Jarcho M., C.H. Bolen, M.B. Thomas, J. Bobick, J.F. Kay & R.H. Doremus, 1976. Hydroxylapatite synthesis and characterization in dense polycrystalline form. J. Mater. Sci. 11, 2027–2035.

Kawasaki T., 1991. Hydroxyapatite as a liquid chromatographic packing. J. Chromatogr. 544, 147–184.

Landi E., A. Tampieri, G. Celotti & S. Sprio, 2000. Densification behaviour and mechanisms of synthetic hydroxyapatites. J. Eur. Ceram. Soc. 20, 2377–2387.

Lim G.K., J. Wang, S.C. Ng & L.M. Gan, 1996. Processing of fine hydroxyapatite powders via an inverse microemulsion route. Mater. Lett. 28, 431–436.

Masuda Y., K. Matsubara & S. Sakka, 1990. Synthesis of hydroxyapatite from metal alkoxides through sol–gel technique. J. Ceram. Soc. Jpn. 98, 1255–1266.

Misra D.N., 1993. Adsorption of low-molecular-weight sodium polyacrylate on hydroxyapatite. J. Dent. Res. 10, 1418–1422.

Okada M. & T. Furuzono, 2006. Nano-sized ceramic particles of hydroxyapatite calcined with an anti-sintering agent. J. Nanosci. Nanotech. (in press).

Papargyris A.D., A.I. Botis & S.A. Papargyri, 2002. Synthetic routes for hydroxyapatite powder production. Key. Eng. Mater. 206–213, 83–86.

Sanchez C. & J. Livage, 1990. Sol–gel chemistry from metal alkoxide precursors. New J. Chem. 14, 513–521.

Schmidt H.K., 2000. Nanoparticles for ceramic and nanocomposite processing. Mol. Cryst. Liq. Cryst. 353, 165–179.

Schmidt H.K., E. Geiter, M. Mennig, H. Krug, C. Becker & R.-P. Winkler, 1998. The sol–gel process for nano-technologies: New nanocomposites with interesting optical and mechanical properties. J. Sol–Gel Sci. Tech. 13, 397–404.

Sindhu S. & S. Valiyaveettil, 2004. Design and synthesis of optically transparent calcium incorporated polymer complex. J. Polym. Sci. B: Polym. Phys. 42, 4459–4465.

Somiya S., K. Ioku & M. Yoshimura, 1988. Hydrothermal synthesis and characterization of fine apatite crystals. Mater. Sci. Forum 34–36, 371–378.

Sonoda K., T. Furuzono, D. Walsh, K. Sato & J. Tanaka, 2002. Influence of emulsion on crystal growth of hydroxyapatite. Solid State Ionics 151, 321–327.

Suchanek W., M. Yashima, M. Kakihana & M. Yoshimura, 1997. Hydroxyapatite/hydroxyapatite-whisker composites without sintering additives: Mechanical properties and microstructural evolution. J. Am. Ceram. Soc. 80, 2805–2813.

Taylor M.G., S.F. Parker, K. Simkiss & P.C.H. Mitchell, 2001. Bone mineral: Evidence for hydroxy groups by inelastic neutron scattering. Phys. Chem. Chem. Phys. 3, 1514–1517.

Yoshida Y., B. Van Meerbeek, Y. Nakayama, M. Yoshioka, J. Snauwaert, Y. Abe, P. Lambrechts, G. Vanherle & M. Okazaki, 2001. Adhesion to and decalcification of hydroxyapatite by carboxylic acids. J. Dent. Res. 80, 1565–1569.

Yoshimura M., H. Suda, K. Okamoto & K. Ioku, 1994. Hydrothermal synthesis of biocompatible whiskers. J. Mater. Sci. 29, 3399–3402.

Zabetakis P.M., C.M. Cotell, D.B. Chrisey & R.C. Auyeung, 1994. Pulsed laser deposition of thin film hydroxyapatite. Applications for flexible catheters. ASAIO J. 40, 869–899.

Preparation of hydroxyapatite-nanocrystals-coated stainless steel, and its cell interaction

Masahiro Okada[1], Miwa Masuda[1], Ryoichi Tanaka[2, 3], Kunio Miyatake[4], Daisuke Kuroda[5], Tsutomu Furuzono[1, *]

[1]Department of Bioengineering, Advanced Medical Engineering Center, National Cardiovascular Center Research Institute, 5-7-1 Fujishirodai, Suita, Osaka 565-8565, Japan

[2]Department of Radiology, National Cardiovascular Center, 5-7-1 Fujishirodai, Suita, Osaka 565-8565, Japan

[3]Present address: Department of Radiology, Iwate Medical University, 19-1 Uchimaru, Morioka, Iwate 020-8505, Japan

[4]National Hospital Organization Osaka Minami Medical Center, 2-1 Kido-higashimachi, Kawachinagano, Osaka 586-8521, Japan

[5]Department of Materials Science and Engineering, Suzuka National College of Technology, Shiroko-cho, Suzuka, Mie 510-0294, Japan

*Author to whom all correspondence should be addressed:

Tel: +81-6-6833-5012 (ext 2623); Fax: +81-6-6872-7485

E-mail: furuzono@ri.ncvc.go.jp

Abstract

Calcined nanocrystals of hydroxyapatite (HAp) having spherical or rod-shaped morphologies were coated through covalent linkage on a Type 316L stainless-steel substrate, which was chemically modified by the graft polymerization of γ-methacryloxypropyl triethoxysilane (MPTS) at 70–110°C. The grafting of poly(MPTS) on the substrate was confirmed by X-ray photoelectron spectroscopy (XPS) and attenuated total reflection Fourier transform infrared spectroscopy (ATR FT-IR). In order to coat the substrate with the HAp crystals through covalent linkage, the reaction between the alkoxysilyl groups in the poly(MPTS) grafted on the substrate and the OH groups on the HAp crystals was conducted at 80°C. The poly(MPTS)-grafted substrate was uniformly and strongly coated with the HAp nanocrystals, although the HAp crystals adsorbed physically on the original substrate without poly(MPTS) grafting were removed by ultrasonic treatment. Human umbilical vein endothelial cells (HUVEC) adhered in larger numbers on the HAp-coated stainless-steel substrate as compared with the original substrate, and spread to a greater extent than that on tissue culture polystyrene (TCPS) after 24 h of initial incubation. The number of HUVEC adhered on the rod-shaped HAp-coated substrate and the spherical HAp-coated substrate at the same HAp coverage ratios of 50% was not significantly different.

Key words

hydroxyapatite – nano-sized crystal – composite – covalent linkage – cell adhesion

1. Introduction

Hydroxyapatite (HAp) ceramics, a type of bioceramics, have been extensively used as implant materials for orthopedic and dental applications because they bond directly to the bone after implantation [1–5], resulting in the formation of a strong bone-implant interface. HAp ceramics have attracted attention also as a soft-tissue compatible material through the development of percutaneous devices [6]. However, owing to their mechanical weakness and brittleness, the applications of HAp ceramics have been confined to those areas for which a low mechanical stress will suffice.

We have recently developed a novel nanocomposite for a soft-tissue-compatible material [7–9]: a silk fibroin or a poly(ethylene terephthalate) fiber, whose surface was modified with nano-sized and calcined HAp crystals through covalent linkage. The novel composite nearly retained the flexibility of the polymer substrate and exhibited good tissue adhesion due to the HAp crystals on its surface [10]. The coating of the calcined HAp nanocrystals may be an effective way to improve the cell- or tissue-adhesion activity of substrates without a coating of adhesion proteins derived from animals, such as collagen and gelatin, which are intractable in terms of sterilization and storage. Recently, there have been also concerns regarding the possible role played by these proteins in infectious diseases such as bovine spongiform encephalopathy (BSE).

If our HAp nanocrystal coating technique can be applied to biomaterials other than polymer materials, its widespread application in medical fields is expected. In this regard, a metal material—Type 316L stainless steel—was selected in this study. Type 316L stainless steel is one of the most important metal biomaterials in the medical field, and has been used in artificial bones

[11], stents [12], etc. The surface modification of metal materials with HAp by the following techniques has been studied with a view to improve biocompatibility: plasma-sprayed coating [13], sputtering coating [14–15], pulsed laser deposition [16], electrochemical deposition [17], electrophoretic deposition [18, 19], treatment with simulated body fluid [20], and sol-gel coating [21]. The HAp-coating layer obtained by the above methods has an amorphous structure or low crystallinity, and the interaction at the interface between HAp and the metal surface is weak [13]. Accordingly, heat treatment around 1000°C is required to crystallize the HAp and obtain stronger interaction between HAp and the metal surface [22]. There is, however, concern regarding the effects of the high-temperature treatment on metal material and the HAp coating layer, e.g., the precipitation of carbide ($Cr_{23}C_6$) and intermetallic phases at the grain boundaries by the heat treatment of Type 316 austenitic stainless steel at 500–900°C [23]; and the metal-catalyzed degradation and shrinkage-induced cracking of the HAp layer [24].

In the present study, the above problems have been overcome by utilizing our novel coating technique for Type 316L stainless-steel substrate with calcined HAp nanocrystals through covalent linkage, which is shown in Fig. 1. The formation of covalent bonding between the HAp nanocrystals and the substrate was carried out at 80°C by a coupling reaction between the OH groups on the HAp crystal and the alkoxysilyl groups of the polymer, which was grafted on the substrate at 70–110°C. The influence of the HAp nanomorphology was evaluated by human umbilical vein endothelial cells (HUVEC) adhesion tests.

Materials and methods

Materials

The Type 316L stainless steel used in this study had a disk shape with a diameter of 12 mm and height of 3 mm, and it had the following bulk composition: C, 0.02%; Ni, 12.12%; Cr, 17.20%; Si, 0.48%; Mn, 1.39%; P, 0.33%; S, 0.24%; Fe, balance. The silane coupling agent, 3-mercaptopropyltrimethoxysilane (95% purity), was purchased from Sigma-Aldrich Co., WI, USA. γ-Methacryloxypropyl trimethoxysilane (MPTS), used as the monomer in the graft polymerization, was donated by Shin-Etsu Chemical Industries Co., Tokyo, Japan. 2,2′-azobis(isobutyronitrile) (AIBN; Nacalai Tesque Inc., Kyoto, Japan), used as the radical initiator, was purified by recrystallization. Water was purified using a Milli-Q system (Millipore Corp., Bedford, Mass.). Other materials were of reagent grade and used as purchased from Nacalai Tesque Inc.

HAp crystals with spherical or rod-shaped morphology were prepared by a wet chemical process. These HAp crystals were used after calcination at 800°C for 1 h with an anti-sintering agent surrounding the crystals to prevent the calcination-induced sintering [25–26]. The agent was removed by washing with water, and then the HAp crystals were dispersed in ethanol medium. The particle sizes measured from scanning electron microscopy (SEM) photographs (see Fig. 2) were as follows: spherical HAp nanocrystals, 73 nm (coefficient of variation (Cv), 23.1%); short axis of rod-shaped crystals, 94 nm (Cv, 26.9%); long axis of rod-shaped crystals, 401 nm (Cv, 50.2%).

Silanization of stainless-steel substrate

First, the stainless-steel substrates were cleaned ultrasonically in an acetone bath for 30 min followed by chemical treatment in a concentrated nitric acid aqueous solution for 30 min. The substrate was then thoroughly rinsed with water, and dried under N_2. The silanization of the substrate was performed at room temperature for 3 h in 10 mM ethanol solution of the silane coupling agent 3-mercaptopropyltrimethoxysilane. The silanized substrate was rinsed with ethanol and water to remove unreacted agents. It was then dried gently in N_2 and aged at 110°C for 1 h.

Graft polymerization of MPTS onto silanized stainless-steel substrate

Graft polymerization of MPTS onto the silanized stainless-steel substrate was conducted according to literature [27] as follows. The substrate was carefully immersed in a 100 mL flask equipped with an inlet for N_2, a reflux condenser, and a stirrer. Anhydrous toluene (25 mL) was added in the flask after purging N_2 for 30 min. The temperature of the mixture was raised to 70°C; 3.3 mL of MPTS monomer and 5 mL of anhydrous toluene solution containing 33 mg of AIBN were then added. The mixture was occasionally stirred during polymerization at 70°C for 2 h. Subsequently, the substrate was washed with ethanol several times to remove any homopolymers that were formed during the polymerization; finally, it was dried under reduced pressure for 1 h at 50°C.

Coating of HAp nanocrystals on stainless-steel substrate

The poly(MPTS)-grafted stainless-steel substrate was soaked in the HAp suspension (1.0 wt%) in ethanol for 1 h at room temperature so that the crystals were adsorbed on the grafted substrate. Then, the substrate was first dried under N_2, and then heated at 80°C for 2 h under vacuum (1 mmHg) in order to form covalent linkage by the reaction between the OH groups on the HAp crystals with the alkoxysilyl groups on the poly(MPTS) grafted on the substrate. The composite was washed in ethanol using an ultra sonic generator (output: 20 kHz and 35 W) for 2 min to remove the unreacted HAp crystals, which were physically adsorbed on other crystals. The composite was finally washed in a large amount of ethanol and water to remove the residual organic compounds.

Cell adhesion test

HUVEC were placed onto the HAp-coated stainless steel in 24-well multiplates at 8×10^4 cells/cm^2 in endothelial cell basal medium-2 (EGM-2; supplemented with heat-inactivated 5% fetal bovine serum (FBS) and 1 mg/mL of gentamicin/amphoterisin B) and incubated at 37°C for 24 h. The original stainless steel and a tissue culture polystyrene (TCPS) dish were used as controls.

For scanning electron microscope (SEM) observation, the samples, after incubation for 24 h, were washed twice in phosphate-buffered saline [PBS(–)]. The cells were then fixed with 10% buffered glutaraldehyde for 20 min at room temperature, followed by rinsing with PBS(–) thrice. The cells were sequentially dehydrated with aqueous ethanol (50–100%) and 100% *n*-butanol for 5 min at room temperature step by step. The samples were lyophilized and coated with gold.

The number of cells that adhered on the samples after incubation for 24 h was counted by colorimetry using Model 680 (Bio-Rad Laboratories, Inc., Tokyo, Japan) at 450 nm after staining with a water-soluble tetrazolium salt (Cell Counting Kit-8; Wako Pure Chemical Industries and Ltd., Osaka, Japan).

Measurements

The surface of the stainless-steel substrates and the cell morphologies were observed using a 5-kV SEM (JSM-6301F, JEOL, Tokyo, Japan). The surface modification of the substrate was confirmed by using attenuated total reflection Fourier transform infrared spectroscopy (ATR FT-IR; Spectrum One, Perkin-Elmer Inc., MA) at 4-cm^{-1} resolution with 16 scans, and X-ray photoelectron spectroscopy (XPS; PHI Model 1600S, Physical Electronics, Inc. MN) with a 100-W non-monochromated MgKα source at an emission angle of 45° and an investigated size of 0.8 × 2.0 mm.

Results and Discussion

A schematic diagram of the procedure for coating the stainless-steel substrate with calcined HAp nanocrystals is shown in Fig. 1. In order to covalently link the substrate and the HAp nanocrystals, the substrate was chemically modified with poly(MPTS), the alkoxysilyl groups of which can couple with the OH groups on the HAp crystal [28]. Although the physical adsorption of the MPTS homopolymer onto a substrate is the simplest method for the modification, it is not the most reliable way to obtain a poly(MPTS)-modified surface, as discussed below. Hence, the